Interlayer coupling and electric field controllable Schottky barriers and contact types in graphene/PbI$_2$ heterostructures

Chuong V. Nguyen [1,*] M. Idrees,[2] Huynh V. Phuc [3] Nguyen N. Hieu,[4]
Nguyen T. T. Binh,[4] Bin Amin [5] and Tuan V. Vu [6,7,†]

[1]*Department of Materials Science and Engineering, Le Quy Don Technical University, Ha Noi 100000, Vietnam*
[2]*Department of Physics, Hazara University, Mansehra 21300, Pakistan*
[3]*Division of Theoretical Physics, Dong Thap University, Cao Lanh 870000, Vietnam*
[4]*Institute of Research and Development, Duy Tan University, Da Nang 550000, Vietnam*
[5]*Abbottabad Uniersity of Science and Technology, Abbottabad 22010, Pakistan*
[6]*Division of Computational Physics, Institute for Computational Science, Ton Duc Thang University, Ho Chi Minh City 700000, Vietnam*
[7]*Faculty of Electrical & Electronics Engineering, Ton Duc Thang University, Ho Chi Minh City 700000, Vietnam*

Van der Waals heterostructures, created by putting graphene on other two-dimensional semiconducting materials, have become an effective strategy to enhance the physical properties and extend the possible applications of two-dimensional (2D) materials. Motivated by the successful synthesis of a graphene/PbI$_2$ heterostructure in a recent experiment [Nat. Commun. **11**, 823 (2020)], here we use first-principles calculations to construct and investigate the electronic properties and interface characteristics of graphene/PbI$_2$ heterostructure. We find that the weak forces occurring at the interface keep heterostructures stable and maintain the intrinsic properties of the constituent graphene and PbI$_2$ monolayers. At the equilibrium interlayer distance of 3.48 Å, the graphene/PbI$_2$ heterostructure forms an *n*-type Schottky contact. More interestingly, the Schottky barrier height and contact types in the graphene/PbI$_2$ heterostructure can be adjusted by electric field and interlayer coupling. The graphene/PbI$_2$ heterostructure can transform from a *n*-type Schottky contact to a *p*-type one or to Ohmic contact by applying electric field or by adjusting interlayer distance. The controllable electronic properties and contact types in graphene/PbI$_2$ heterostructure make it a promising candidate for designing and improving the performance of high-efficiency Schottky nanodevices.

I. INTRODUCTION

In the past decade, the successful exfoliation of graphene [1] has opened a door to the world of novel two-dimensional (2D) materials. To date, a plethora of different 2D materials, such as hexagonal boron nitride (*h*-BN) [2,3], phosphorene [4,5], transition-metal dichalcogenides (TMDs) [6–8], silicene [9,10], germanene [11,12], and so forth, have been fabricated and confirmed as potential candidate for novel applications, including field-effect transistors (FETs) [13,14] and photodetectors [15,16]. Unfortunately, these 2D materials in their single form contain some drawbacks that are not desirable for high-performance electronic and optoelectronic devices. For instance, the lack of a band gap in graphene hinders its application in high-speed FET [17]. Monolayer MoS$_2$, one of the TMD family, exhibits a semiconductor nature with a band gap of about 2 eV [18]. However, the low carrier mobility of MoS$_2$ monolayer limits its application applications in nanoelectronics [19]. Phosphorene, a type of 2D material, possesses high carrier mobility, especially for

holes [20]. However, the instability of phosphorene under ambient conditions has limited its application in modern day devices.

Recently, constructing layered van der Waals (vdW) heterostructures (HTSs) by putting a 2D material on top of another one has been experimentally and theoretically confirmed to be one of the most effective strategies to enhance the electronic properties and optical performances of 2D materials [21,22]. Nowadays, there are already numerous theoretical and experimental efforts to investigate 2D layered vdW-HTSs, especially graphene-based vdW-HTSs, such as graphene/TMDs [23–26], graphene/phosphorene [27–29], graphene/GaS(Se) [30–34], graphene/GeC [35,36], and so forth. One can find that in the graphene-based vdW-HTSs, the weak vdW forces between graphene and other 2D materials keep the HTSs feasible and preserve the intrinsic electronic and optical properties of the constituent materials. Moreover, the graphene-based vdW-HTSs exhibit many properties which are desirable for designing and enhancing the performances of electronic and nanoelectronic devices. For instance, Aziza *et al.* [32] experimentally fabricated graphene/GaSe HTS using molecular beam epitaxy (MBE) and demonstrated that the graphene/GaSe HTS can use for future nanoelectronic and optoelectronic devices, which require a high photoresponse.

*chuongnguyen11@gmail.com
†Corresponding author: vuvantuan@tdtu.edu.vn

On the other hand, Kim *et al.* [34] reported a FET based on graphene/GaSe heterojunction with high photoresponsivity of about 10 mA/W. Si *et al.* [31] used first-principles calculations to demonstrate that the tunable band alignment and contact types in graphene/GaSe HTS can enhance its potential applications in electronic and optoelectronic devices.

Very recently, Sinha and coworkers [37] successfully synthesized the graphene/PbI$_2$ vdW heterostructure by exfoliation. They found that the vdW forces between graphene and PbI$_2$ layer tends to the formation of the 1H crystal phase of PbI$_2$. It should be noted that the single crystal of PbI$_2$ has been experimentally synthesized using a hydrothermal strategy [38]. Monolayer PbI$_2$ exhibits a natural semiconductor with an indirect band gap of 2.5 eV, which can be effectively controlled by powerful strategies as biaxial strains [39] and thickness layers [40]. The controllable electronic properties of monolayer PbI$_2$ make it promising candidate for photoluminescence and optical field applications. Theoretically, Zhou *et al.* [39] have constructed the graphene/PbI$_2$ HTS and demonstrated that the visible light absorption can be enhanced as compared to monolayer PbI$_2$. However, the graphene/PbI$_2$ HTS exhibits a large lattice mismatch of about 8%, which may affect strongly the intrinsic electronic properties of such HTS, which has not been considered in previous works.

Therefore, in this work, using first-principles calculations, we investigate systematically the electronic properties and interface characteristics of graphene/PbI$_2$ HTS. The weak vdW interactions between graphene and PbI$_2$ layer makes the graphene/PbI$_2$ HTS feasible and can be synthesized in recent experiments [37]. Moreover, at the equilibrium state, graphene/PbI$_2$ forms a *n*-type Schottky contact that can be switched to a *p*-type or Ohmic contact under strain and electric field. Our work is organized as follows: Details of the computational methodology are provided in Sec. II. The band alignment and contact types of graphene/PbI$_2$ heterostructure along with the effects of strain and electric field are discussed and presented in Sec. III.

II. COMPUTATIONAL DETAILS

First-principle calculations with the QUANTUM ESPRESSO package [41,42] have been performed to calculate the structural, electronic, and optical properties of the constituent monolayers and their corresponding vdW heterostructures. A plane-wave basis set and projector augmented wave (PAW) pseudopotentials [43] are used along with density functional theory. The exchange correlation function is approximated by the generalized gradient approximation of Perdew, Burke, and Ernzerhof (PBE) [44]. To describe correctly the weak forces in layered materials, the DFT-D3 method [45] by adding a semiempirical dispersion potential to the traditional DFT method is adopted for all calculations. The cutoff energy is set to be 510 eV and a $(9 \times 9 \times 1)$ k-point grid of the first Brillouin zone (BZ) was performed for Monkhorst-Pack mesh [46]. In order to break unphysical interactions between periodic images of systems, a large vacuum of 30 Å is applied along the z direction. The convergence criterion of energy in the self-consistency process is set to be 10^{-6} eV. All the geometric optimization processes were obtained when the Hellmann-Feynman forces on atoms are smaller than

0.01 eV/Å. Moreover, the dipole corrections are also added in our calculations in order to examine the charge transfer and charge redistribution in the heterostructure.

The *ab initio* molecular dynamics simulations (AIMD) [47] is used to confirm the thermal stability of graphene/PbI$_2$ heterostructure. AIMD simulations are performed through Nose-thermostat algorithm at temperature of 300 K for total 6 ps with a time step of 1 fs.

III. RESULTS AND DISCUSSION

We first examine the structural and electronic characteristics of both graphene and PbI$_2$ monolayers for their unit cell. These results are depicted in Fig. 1. At the ground state, graphene possesses a metallic nature, whereas monolayer PbI$_2$ exhibits a semiconducting behavior. The lattice parameters of graphene and PbI$_2$ in their unit cell are 2.46 and 4.72 Å, respectively, which are consistent with previous reports [39], confirming the reliability of our computational methods. It is clear that the PbI$_2$ monolayer has the hexagonal crystal, where one Pb atom is sandwiched between two I atoms in both sides. Phonon dispersion curves of both graphene and PbI$_2$ monolayers are depicted in Fig. 1(c). It is clear that graphene and PbI$_2$ monolayers for their unit cell are dynamical stable with no soft modes in the phonon spectrum.

The difference in the lattice parameters of graphene and PbI$_2$ monolayers leads us to use a supercell to build the graphene/PbI$_2$ HTS. The supercell contains of a (2×2) PbI$_2$ supercell and (4×4) graphene supercell. The lattice mismatch between graphene and PbI$_2$ layers in their corresponding HTS is small, 2.1%, which will have no affect the electronic properties of HTS. The graphene/PbI$_2$ HTS have different stacking configurations, and the most energetically favorable stacking configuration is depicted in Fig. 2(a) and 2(b). At the equilibrium state, the interlayer distance (D_{eq}) between graphene layer and topmost I layer is calculated to be 3.48 Å, which is consistent with other typical vdW graphene-based HTS, such as graphene/MoS$_2$ [48], graphene/SnS [49], and graphene/phosphorene [27]. This indicates that with such value of the D_{eq} the graphene/PbI$_2$ HTS is mainly characterized by the weak vdW forces, occurring between graphene and the topmost I layer.

Furthermore, to determine the structural stability of HTS, we examine its binding energy, which can be calculated as the difference in the total energies of HTS (E_{HTS}) and corresponding monolayers (E_{M}): $E_{\text{b}} = (E_{\text{HTS}} - \sum E_{\text{M}}]/A$, where A is the in-plane surface area of HTS. Our obtained E_{b} of graphene/PbI$_2$ is -10.04 meV/Å^2. The negative value of the binding energy confirms that such HTS is feasible and thus it can be easily realized in experiments. Moreover, this value of E_{b} in graphene/PbI$_2$ HTS is comparable with that in other vdW graphene-related systems, such as graphite [50] and *h*-BN [51]. It also confirms that graphene and PbI$_2$ layers are bonded to each other via the weak vdW forces, and thus the graphene/PbI$_2$ HTS can be synthesized experimentally by the exfoliation method [37]. Furthermore, to examine the thermal stability of the most energetically favorable stacking configuration of graphene/PbI$_2$, we next perform *ab initio* molecular dynamics (AIMD) simulation at room temperature (300 K). The fluctuation of total energy as a function of
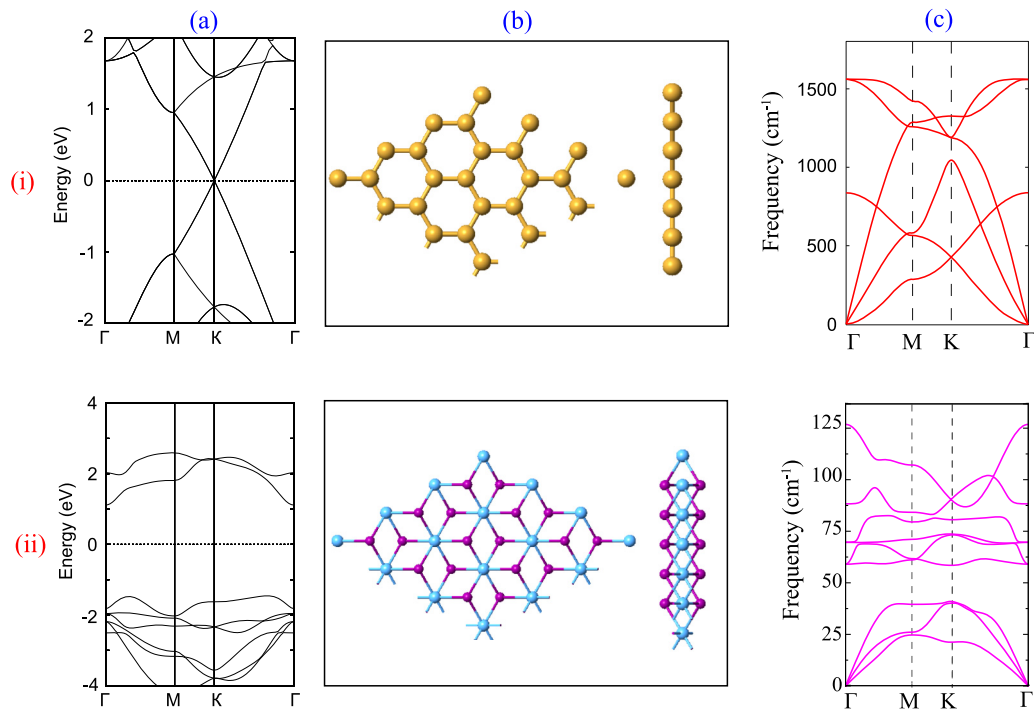
FIG. 1. (a) Band structure, (b) atomic structure, and (c) phonon spectrum of (i) graphene and (ii) PbI$_2$ monolayers, respectively.

time step is depicted in Fig. 3. One can observe from the snapshot of graphene/PbI$_2$ HTS after 6 ps that there are no structure distortion. Moreover, the fluctuation of the total energies as a function of time step is small. Moreover, through the AIMD simulation, our results demonstrate that the geometrical structure of graphene/PbI$_2$ HTS is well kept after 6000 step simulations, and the average value of total energy remains nearly constant during the entire simulation. All these

findings demonstrate that the graphene/PbI$_2$ HTS is thermally stable at room temperature.

The projected band structures of isolated graphene, PbI$_2$ monolayers, and graphene/PbI$_2$ HTS are depicted in Fig. 4. When the graphene and PbI$_2$ layers are stacked together to form graphene/PbI$_2$ HTS, it is clear that they are bonded to each other via the vdW interactions as mentioned above. This interaction keeps the graphene/PbI$_2$ HTS stable and thus it results on the preservation in the band structures of both graphene and PbI$_2$ monolayers. One can find from Figs. 4(a)–4(c) that the band structure of such HTS is the sum of that of graphene and PbI$_2$ monolayers. The values of the band gap of isolated graphene and PbI$_2$ layers are calculated to be 5 meV and 2.46 eV, respectively. It indicates that the combination of graphene and PbI$_2$ monolayers results in the
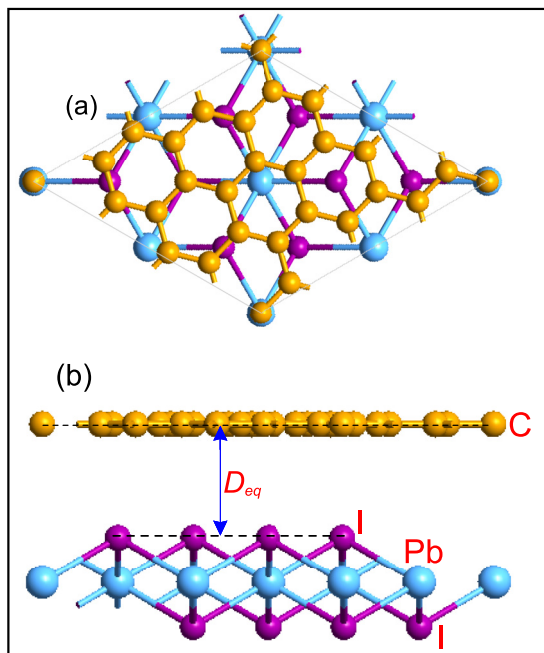
FIG. 2. (a) Top view and (b) side view of the most energetically favorable graphene/PbI$_2$ HTS.
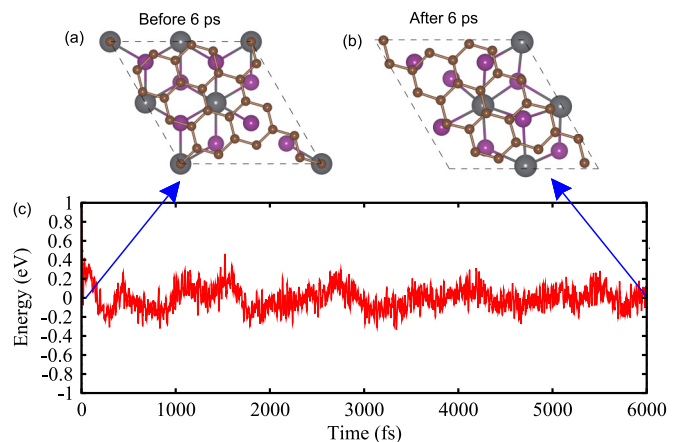
FIG. 3. Snapshots of structure of graphene/PbI$_2$ HTS (a) before and (b) after heating 6 ps. (c) The AIMD simulation of the fluctuation in energy as a function of time step of graphene/PbI$_2$ HTS.
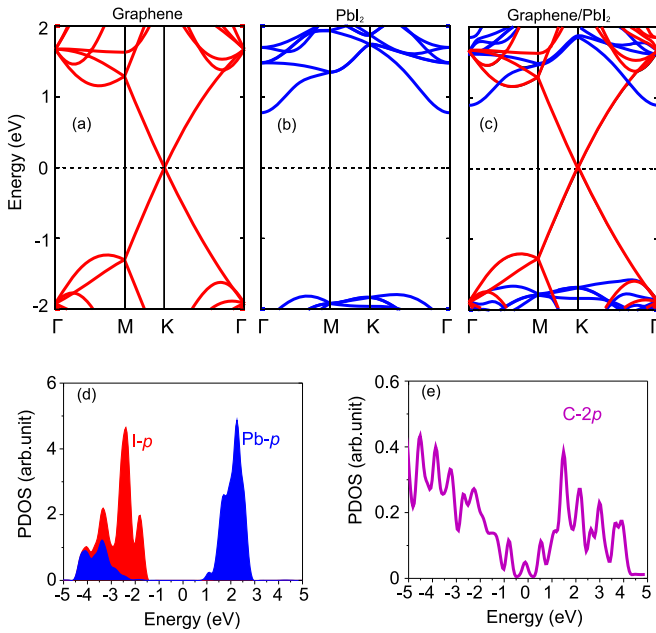
FIG. 4. Calculated band structures of (a) isolated graphene, (b) PbI$_2$ monolayer, and (c) graphene/PbI$_2$ HTS. The dashed line represents the Fermi level, which is set to be zero. The partial density of states (PDOS) of (d) PbI$_2$ part and (e) graphene layer in their corresponding HTS.

FIG. 5. (a) Electrostatic potential and (b) band alignment of graphene/PbI$_2$ HST. (c) Schematic model of FET based on graphene/PbI$_2$ HTS. The inset in panel (a) is the charge density difference of the graphene/PbI$_2$ HTS. The yellow and cyan regions represent the charge accumulation and depletion, respectively.

formation of a band gap opening in graphene. This small band gap opening in graphene demonstrates that the graphene/PbI$_2$ HTS will have a high carrier mobility as compared with perfect graphene. Furthermore, to have a better insight into the electronic properties of such graphene/PbI$_2$ HTS, we plot their partial density of states (PDOS), as depicted in Figs. 4(c) and 4(d). One can see that the Dirac cone around the Fermi level is created by the C-2p orbitals in graphene, while the VBM and CBM of the PbI$_2$ part come from the I-p and Pb-p orbitals, respectively.

In order to understand this charge-transfer trend and charge redistribution in graphene/PbI$_2$ HTS, we further calculate the charge density difference as follows: $\Delta\rho = \rho_{\mathrm{HTS}} - \sum \rho_{\mathrm{M}}$, where ρ_{HTS} and ρ_{M} are the charge density of the HTS and the monolayers. These results are presented in the inset of Fig. 5(a). One can see that the charges are mainly depleted in the graphene layer, whereas they are accumulated in the PbI$_2$ layer, leading to a transfer for the charges from graphene to the PbI$_2$ layer. Moreover, one can observe from Fig. 5(a) that the graphene layer has a deeper potential than that of the PbI$_2$ layer, resulting in the formation of a large potential drop, which suggests a strong electrostatic field across the heterostructure. When the graphene layer is used as an electrode, this strong electrostatic field will exhibit strong effects on the carrier dynamics and induce a low charge-injection barrier, which will facilitate charge injection, resulting in better device performance. Obviously, a dipole moment (*P*) can be calculated as $P = \Delta Q \times D_{\mathrm{eq}}$. To quantify the charge transfer, we perform a Bader analysis [52], which demonstrates that only 0.054 electrons are transferred from graphene to the PbI$_2$ layer. Although the interactions between graphene and PbI$_2$ are weak and there are only small amounts of charge transfers
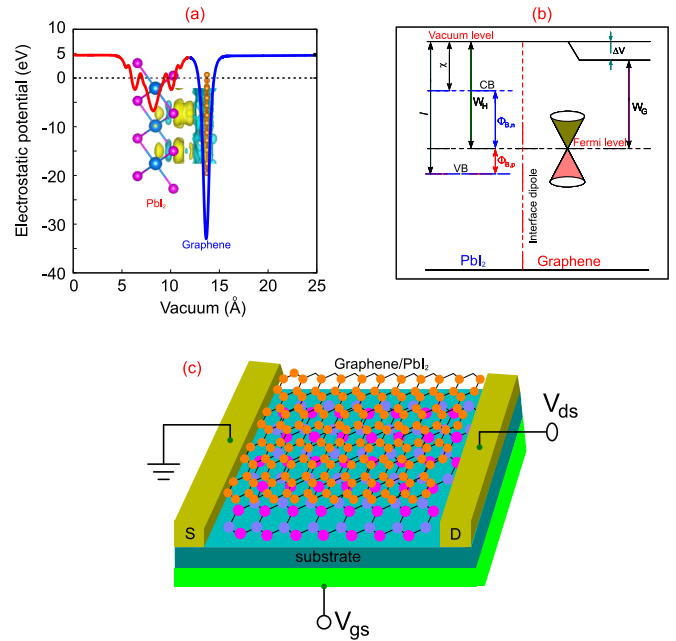
between them, it leads to the formation of a interface dipole with a large potential step, as shown in Fig. 5(b). This observation was confirmed by experiments in other graphene-based HTS, such as graphene/GaSe [32] and graphene/MoS$_2$ [25]. Moreover, the plane averaged electrostatic potential across the interface is also considered. The ionization potential (*I*) is given from the vacuum energy level (E_{vac}), which is defined as $I = E_{\mathrm{vac}} - E_{\mathrm{VBM}}$, where E_{vac} refers to the vacuum potential. Our calculated *I* value of the graphene/PbI$_2$ HTS is 4.8 eV. The calculated potential drop ΔV across the graphene/PbI$_2$ HTS is 28 eV. A comparatively large potential drop is found in graphene/PbI$_2$ HTS, suggesting a considerably strong electrostatic field. The deeper potential is caused by the different atomic electronegativity of Pb, I, and C atoms. Furthermore, to confirm the charger transfer in the graphene/PbI$_2$ HTS, we calculate the work functions of the constituent graphene and PbI$_2$ monolayers, which are calculated to be 4.25 and 5.87 eV, respectively. Because of the large difference in the work functions between graphene and PbI$_2$ monolayers, electrons will spontaneously flow from graphene into PbI$_2$ layer. These results demonstrate that the graphene/PbI$_2$ can be considered as a promising candidate for high-efficiency FET, as depicted in Fig. 5(c). It should be noted that the preliminary requirement for application of graphene/PbI$_2$ HTS in high-performance FET device is that its carrier mobility should be high. Moreover, the carrier mobility relates to the effective masses in following relationship: $\mu = e\tau/m^*$. Therefore, to clarify the carrier mobility of graphene/PbI$_2$ HTS, we calculate the effective masses for electrons and holes as follows:

$$\frac{1}{m^*} = \frac{1}{\hbar}\frac{\partial^2 E(k)}{\partial k^2}. \tag{1}$$
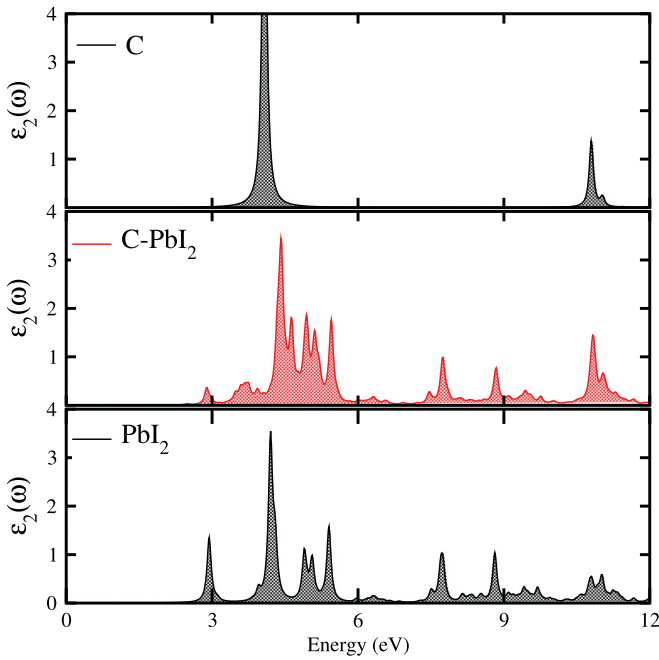
FIG. 6. Imaginary part of dielectric functions of graphene/PbI$_2$ HTS along with that of isolated graphene and PbI$_2$ monolayers.

FIG. 7. The variation of the SBH of graphene/PbI$_2$ HTS as a function of electric fields.

Here, $\hbar$ is the Planck constant and k is the wave vector. The effective masses for electrons and holes are 7.63×10^{-3} m$_0$ and 5.23×10^{-3} m$_0$, respectively. The small effective mass of graphene/PbI$_2$ demonstrates that it has high carrier mobility, which merits high-speed FET, as depicted in Fig. 5(c).

The optical absorption behaviors of graphene, PbI$_2$, and the graphene/PbI$_2$ HTS are also calculated and depicted in Fig. 6. It is found that PbI$_2$ and graphene have one absorption peak at 2.8 and 3.2 eV in the visible light region, and there are several peaks at the ultraviolet region while the graphene/PbI$_2$ HTS has one peak at 2.7 eV. It can be clearly seen that such heterostructures possess high-performance absorption in the visible and near-infrared regions, indicating that it is useful for acquiring efficient photocatalysts. Moreover, one can observe that the red shift was observed in the graphene/PbI$_2$ heterostructure.

More interestingly, when graphene is placed on the PbI$_2$, it tends to the formation of the metal-semiconductor heterojunction, which is characterized by Schottky or Ohmic contact. Based on the Schottky-Mott rule [53], both the n-type Schottky barrier (Φ_n) and p-type Schottky barrier (Φ_p) can be defined as $\Phi_n = E_{CB} - E_F$ and $\Phi_p = E_F - E_{VB}$. It is clear from Fig. 4(c) that the Fermi level of such HTS is closer to the CBM of PbI$_2$ layer, leading to the formation of n-type semiconductor. The band gap E_g of the PbI$_2$ semiconductor in the graphene/PbI$_2$ HTS can be obtained as $E_g = E_{CB} - E_{VB}$, i.e., $E_g = \Phi_n - \Phi_p$. According to the Schottky-Mott rule, our calculated Φ_n and Φ_p are 0.89 and 1.57 eV, respectively. It indicates that the graphene/PbI$_2$ HTS forms the n-type Schottky contact (n-SC) at the equilibrium state. Moreover, the switchable Schottky barrier (SB) and contact types in the graphene/PbI$_2$ HTS is crucial for fabricating its future high-performance Schottky devices. Therefore, it is important to examine whether the SBH and contact types of the
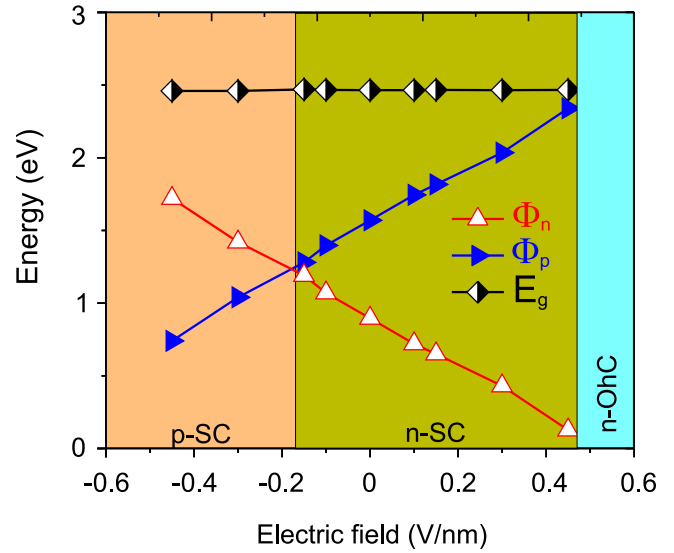
graphene/PbI$_2$ HTS can be tuned. Previously, many studies have been reported that both the SBH and contact types in graphene-based HTS can be effectively modulated by interlayer distance and external electric field [31,35,36,54].

We first examine the controllable electronic properties and contact types of graphene/PbI$_2$ HTS under external electric fields ($E_\perp$), which are applied along the z direction of the heterostructure. The direction of electric field, pointing from graphene to the PbI$_2$ layer, is defined by the positive. The changes in the SBH and contact types of graphene/PbI$_2$ HTS under $E_\perp$ are illustrated in Fig. 7. One can find that the negative $E_\perp$ (n-$E_\perp$) results in an increase in the Φ_n and a decrease in the Φ_p. When n-$E_\perp > -0.17$ V/nm, one can find that the graphene/PbI$_2$ HTS keeps the n-type Schottky contact (n-SC) contact because the Φ_n is still smaller than the Φ_p. When the n-$E_\perp$ is continuously decreased, i.e., n-$\Phi_n \leqslant -0.17$ V/nm, we find that the Φ_p is continuously decreased and becomes smaller than the Φ_n, converting the graphene/PbI$_2$ HTS from n-SC to p-type Schottky contact (p-SC). It indicates that the n-$E_\perp$ can transform the graphene/PbI$_2$ HTS from n-SC to p-SC. In contract to the n-$E_\perp$, the positive (p) $E_\perp$ leads to the narrower Φ_n and wider Φ_p. It suggests that the graphene/PbI$_2$ HTS still keeps the n-SC under the p-$E_\perp$. More interestingly, when the p-$E_\perp$ is higher than $+0.5$ V/nm, the Φ_n is narrowed to approximately zero. It indicates that the p-$E_\perp$ can transform the graphene/PbI$_2$ HTS from n-SC to n-type Ohmic contact (n-OC).

In order to have a deep understanding of the electric-field-tunable electronic properties of graphene/PbI$_2$ HTS, we calculate its projected band structures under different n-$E_\perp$ and p-$E_\perp$. These results are depicted in Fig. 8. One can find that the Fermi level of graphene/PbI$_2$ HTS moves toward the VBM of the PbI$_2$ part under the n-$E_\perp$. It means that under the n-$E_\perp$ the VBM of the PbI$_2$ part moves closer to the Fermi level, whereas the CBM shifts far from the Fermi level. Therefore, under the n-$E_\perp$, the Φ_n is widened, while the Φ_p is narrowed. When the n-$E_\perp$ is smaller than -0.17 V/nm,
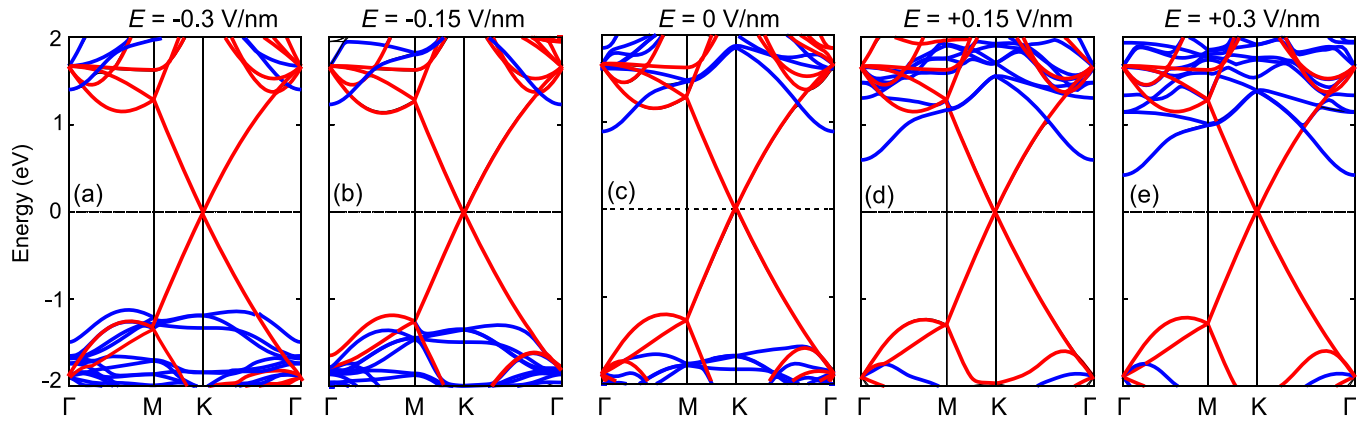
FIG. 8. Projected band structures of graphene/PbI$_2$ HTS under different strengths of electric fields, ranging from (a) $E = -0.3$ V/nm, (b) $E = -0.15$ V/nm, (c) $E = 0$ V/nm, (d) $E = +0.15$ V/nm, and (e) $E = +0.3$ V/nm. The dashed line represents the Fermi level, which is set to be zero. Red and blue lines represent the contributions of the graphene and PbI$_2$ layers, respectively.

the VBM of the PbI$_2$ part is closer to the Fermi level than its CBM, leading to a transformation from n-SC to p-SC in the graphene/PbI$_2$ HTS. In contrast to the case of the n-$E_\perp$, the Fermi level of graphene/PbI$_2$ HTS moves toward the CBM of the PbI$_2$ part. This nature leads to an increase in the Φ_n and to a decrease in the Φ_p and thus results in the transformation from n-SC to n-OC at the critical p-$E_\perp$ of +0.5 V/nm.

The dependence of the binding energy, SBH, and contact types of graphene/PbI$_2$ HTS as a function of interlayer distances is illustrated in Fig. 9. Before investigating this effect, it should be noted that the interlayer couplings in vdW heterostructures can adjust in experiments through different strategies, including scanning tunnel microscopy [55] and the insertion of hexagon boron nitride [56]. Figure 9(a) shows that the graphene/PbI$_2$ HTS has the lowest binding energy at the equilibrium interlayer distance of $D_{eq} = 3.48$ Å. It is interesting from Fig. 9(b) that the interlayer coupling can be used to modify both the SBH and the contact types of such graphene/PbI$_2$ HTS. Indeed, one can find from Fig. 9 that the SBHs of graphene/PbI$_2$ HTS, including Φ_n and Φ_p, vary by two different ways. The Φ_n is decreased with increasing the interlayer distance, while the Φ_p is increased with increasing the interlayer distance. It is obvious from Fig. 9(b) that when the interlayer distance is smaller than 3.0 Å, the Φ_p decreases and becomes smaller than the Φ_n of graphene/PbI$_2$ HTS, leading to the transformation from n-SC to p-SC contact.

The band structures of graphene/PbI$_2$ HTS under different interlayer distances are also calculated and depicted in Fig. 10. It can be seen that when the interlayer distance is increased, the Fermi level moves toward the CBM of PbI$_2$ part. Thus, the Φ_n of such HTS is decreased, whereas its Φ_p decreases with increasing the interlayer distance. When the interlayer distance is smaller than 3.0 Å, the VBM of PbI$_2$ part gets closer to the Fermi level than the CBM, thus making a transition from n-SC to p-SC contact type. The nature of the strain effects on electronic properties of graphene/PbI$_2$ HTS is related to the charge transfer between two constituent monolayers. Bader charge analysis shows that the charge transfers from graphene to PbI$_2$ layers at the interlayer spacing of 3.48, 3.08, and 2.68 Å are 0.054, 0.062, and 0.071 e, respectively. It indicates that with decreasing the interlayer spacing, the interlayer coupling between graphene and PbI$_2$ is enhanced, and thus more electrons are transferred from graphene to the PbI$_2$ layer. When the interlayer coupling is strengthened, i.e., the interlayer distance decreases, more electrons are transferred from graphene to VBM of the PbI$_2$
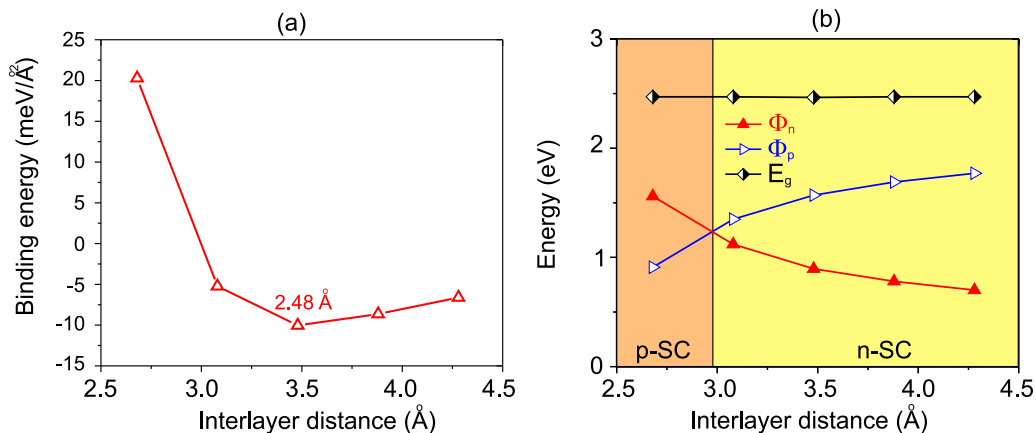
FIG. 9. The variation of (a) binding energy and (b) the SBH of graphene/PbI$_2$ HTS as a function of interlayer distances.
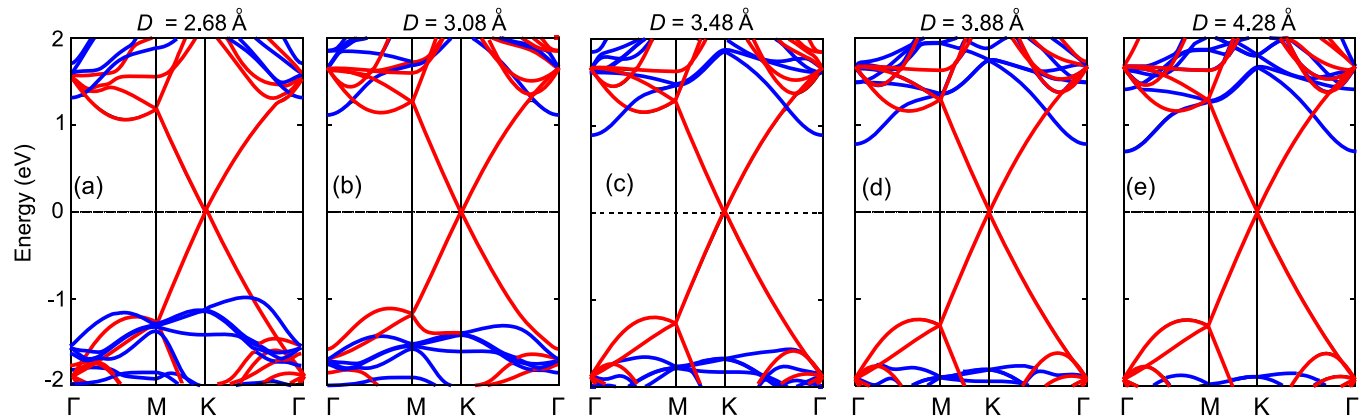
FIG. 10. Projected band structures of graphene/PbI$_2$ HTS under different interlayer spacings: (a) $D = 2.68$ Å, (b) $D = 3.08$ Å, (c) $D = 3.48$ Å, (d) $D = 3.88$ Å, and (e) $D = 4.28$ Å. The dashed line represents the Fermi level, which is set to be zero. Red and blue lines represent the contributions of the graphene and PbI$_2$ layers, respectively.

layer, leading to a decrease in the Φ_p. The controllable SBH and contact types in graphene/PbI$_2$ HTS make it promising candidate for designing the Schottky devices.

IV. CONCLUSION

In conclusion, we have constructed theoretically and investigated systematically the structural, electronic properties, and interface characteristics of graphene/PbI$_2$ heterostructure using first-principles calculations. The combination between graphene and PbI$_2$ monolayer tends to the formation of the n-type Schottky contact with the Schottky barrier height of 0.89 eV. The weak vdW forces keeps the graphene/PbI$_2$ heterostructure feasible and can be synthesized in experiments. The intrinsic electronic properties of both graphene and PbI$_2$ monolayers are well preserved in such heterostructure. Furthermore, the strain engineering and electric field are crucial for controlling both the Schottky barrier height and contact

types of graphene/PbI$_2$ heterostructure. The graphene/PbI$_2$ heterostructure can transform from the n-type Schottky contact to the p-type one or to Ohmic contact by applying electric field or by adjusting interlayer distance. The controllable electronic properties and contact types in graphene/PbI$_2$ HTS make it a promising candidate for designing and improving the performance of high-efficiency Schottky nanodevices.

The authors declare that there are no conflicts of interest regarding the publication of this paper.

[1] K. S. Novoselov, A. K. Geim, S. V. Morozov, D. Jiang, Y. Zhang, S. V. Dubonos, I. V. Grigorieva, and A. A. Firsov, Science **306**, 666 (2004).

[2] S. Reich, A. C. Ferrari, R. Arenal, A. Loiseau, I. Bello, and J. Robertson, Phys. Rev. B **71**, 205201 (2005).

[3] G. Cassabois, P. Valvin, and B. Gil, Nat. Photon. **10**, 262 (2016).

[4] E. S. Reich, Nature (London) **506**, 19 (2014).

[5] A. Carvalho, M. Wang, X. Zhu, A. S. Rodin, H. Su, and A. H. C. Neto, Nat. Rev. Mater. **1**, 1 (2016).

[6] Q. H. Wang, K. Kalantar-Zadeh, A. Kis, J. N. Coleman, and M. S. Strano, Nat. Nanotechnol. **7**, 699 (2012).

[7] D. Jariwala, V. K. Sangwan, L. J. Lauhon, T. J. Marks, and M. C. Hersam, ACS Nano **8**, 1102 (2014).

[8] S. Manzeli, D. Ovchinnikov, D. Pasquier, O. V. Yazyev, and A. Kis, Nat. Rev. Mater. **2**, 17033 (2017).

[9] P. Vogt, P. De Padova, C. Quaresima, J. Avila, E. Frantzeskakis, M. C. Asensio, A. Resta, B. Ealet, and G. Le Lay, Phys. Rev. Lett. **108**, 155501 (2012).

[10] N. D. Drummond, V. Zólyomi, and V. I. Fal'ko, Phys. Rev. B **85**, 075423 (2012).

[11] A. Acun, L. Zhang, P. Bampoulis, M. Farmanbar, A. van Houselt, A. Rudenko, M. Lingenfelder, G. Brocks, B. Poelsema, M. Katsnelson, and H. Zandvliet, J. Phys.: Condens. Matter **27**, 443002 (2015).

[12] M. Dávila, L. Xian, S. Cahangirov, A. Rubio, and G. Le Lay, New J. Phys. **16**, 095002 (2014).

[13] A. Nourbakhsh, A. Zubair, R. N. Sajjad, A. Tavakkoli KG, W. Chen, S. Fang, X. Ling, J. Kong, M. S. Dresselhaus, E. Kaxiras, K. K. Berggren, A. Dimitri, and T. Palacios, Nano Lett. **16**, 7798 (2016).

[14] M. Z. Rahman, C. W. Kwong, K. Davey, and S. Z. Qiao, Energy Environ. Sci. **9**, 709 (2016).

[15] S. Li, T. Wang, X. Chen, W. Lu, Y. Xie, and Y. Hu, Nanoscale **10**, 7694 (2018).

[16] S. Alkis, T. Öztaş, L. Aygün, F. Bozkurt, A. Okyay, and B. Ortaç, Opt. Express **20**, 21815 (2012).

[17] A. H. Castro Neto, F. Guinea, N. M. R. Peres, K. S. Novoselov, and A. K. Geim, Rev. Mod. Phys. **81**, 109 (2009).

[18] K. F. Mak, C. Lee, J. Hone, J. Shan, and T. F. Heinz, Phys. Rev. Lett. **105**, 136805 (2010).

[19] B. Radisavljevic, A. Radenovic, J. Brivio, V. Giacometti, and A. Kis, Nat. Nanotechnol. **6**, 147 (2011).

[20] A. Peruzzo, J. McClean, P. Shadbolt, M.-H. Yung, X.-Q. Zhou, P, J. Love, A. Aspuru-Guzik, and J. L. O'Brien, Nat. Commun. **5**, 4213 (2014).

[21] S. Das, J. A. Robinson, M. Dubey, H. Terrones, and M. Terrones, Annu. Rev. Mater. Res. **45**, 1 (2015).

[22] Y. Liu, Y. Huang, and X. Duan, Nature (London) **567**, 323 (2019).

[23] H. Henck, Z. Ben Aziza, D. Pierucci, F. Laourine, F. Reale, P. Palczynski, J. Chaste, M. G. Silly, F. Bertran, P. Le Fèvre, E. Lhuillier, T. Wakamura, C. Mattevi, J. E. Rault, M. Calandra, and A. Ouerghi, Phys. Rev. B **97**, 155421 (2018).

[24] Z. B. Aziza, H. Henck, D. Di Felice, D. Pierucci, J. Chaste, C. H. Naylor, A. Balan, Y. J. Dappe, A. C. Johnson, and A. Ouerghi, Carbon **110**, 396 (2016).

[25] D. Pierucci, H. Henck, J. Avila, A. Balan, C. H. Naylor, G. Patriarche, Y. J. Dappe, M. G. Silly, F. Sirotti, A. C. Johnson, M. C. Asensio, and A. Ouerghi, Nano Lett. **16**, 4054 (2016).

[26] N. N. Hieu, H. V. Phuc, V. V. Ilyasov, N. D. Chien, N. A. Poklonski, N. Van Hieu, and C. V. Nguyen, J. Appl. Phys. **122**, 104301 (2017).

[27] J. E. Padilha, A. Fazzio, and A. J. R. da Silva, Phys. Rev. Lett. **114**, 066803 (2015).

[28] H. V. Phuc, V. V. Ilyasov, N. N. Hieu, and C. V. Nguyen, Vacuum **149**, 231 (2018).

[29] S. Liu, Z. Li, Y. Ge, H. Wang, R. Yue, X. Jiang, J. Li, Q. Wen, and H. Zhang, Photon. Res. **5**, 662 (2017).

[30] H. V. Phuc, N. N. Hieu, B. D. Hoi, and C. V. Nguyen, Phys. Chem. Chem. Phys. **20**, 17899 (2018).

[31] C. Si, Z. Lin, J. Zhou, and Z. Sun, 2D Mater. **4**, 015027 (2016).

[32] Z. Ben Aziza, H. Henck, D. Pierucci, M. G. Silly, E. Lhuillier, G. Patriarche, F. Sirotti, M. Eddrief, and A. Ouerghi, ACS Nano **10**, 9679 (2016).

[33] K. D. Pham, N. N. Hieu, H. V. Phuc, I. Fedorov, C. Duque, B. Amin, and C. V. Nguyen, Appl. Phys. Lett. **113**, 171605 (2018).

[34] W. Kim, S. Arpiainen, H. Xue, M. Soikkeli, M. Qi, Z. Sun, H. Lipsanen, F. A. Chaves, D. Jimenez, and M. Prunnila, ACS Appl. Nano Mat. **1**, 3895 (2018).

[35] X. Gao, Y. Shen, Y. Ma, S. Wu, and Z. Zhou, Comput. Mater. Sci. **170**, 109200 (2019).

[36] S. Wang, J.-P. Chou, C. Ren, H. Tian, J. Yu, C. Sun, Y. Xu, and M. Sun, Sci. Rep. **9**, 1 (2019).

[37] S. Sinha, T. Zhu, A. France-Lanord, Y. Sheng, J. C. Grossman, K. Porfyrakis, and J. H. Warner, Nat. Commun. **11**, 823 (2020).

[38] X. Zhu, P. Wangyang, H. Sun, D. Yang, X. Gao, and H. Tian, Mater. Lett. **180**, 59 (2016).

[39] M. Zhou, W. Duan, Y. Chen, and A. Du, Nanoscale **7**, 15168 (2015).

[40] M. Yagmurcukardes, F. M. Peeters, and H. Sahin, Phys. Rev. B **98**, 085431 (2018).

[41] P. Giannozzi, S. Baroni, N. Bonini, M. Calandra, R. Car, C. Cavazzoni, D. Ceresoli, G. L. Chiarotti, M. Cococcioni, I. Dabo, A. D. Corso, S. de Gironcoli, S. Fabris, G. Fratesi, R. Gebauer, U. Gerstmann, C. Gougoussis, A. Kokalj, M. Lazzeri, L. Martin-Samos, N. Marzari, F. Mauri, R. Mazzarello, S. Paolini, A. Pasquarello, L. Paulatto, C. Sbraccia, S. Scandolo, G. Sclauzero, A. P. Seitsonen, A. Smogunov, P. Umari, and R. M. Wentzcovitch, J. Phys.: Condens. Matter **21**, 395502 (2009).

[42] P. Giannozzi, O. Andreussi, T. Brumme, O. Bunau, M. B. Nardelli, M. Calandra, R. Car, C. Cavazzoni, D. Ceresoli, M. Cococcioni, N. Colonna, I. Carnimeo, A. D. Corso, S. de Gironcoli, P. Delugas, R. A. DiStasio, A. Ferretti, A. Floris, G. Fratesi, G. Fugallo, R. Gebauer, U. Gerstmann, F. Giustino, T. Gorni, J. Jia, M. Kawamura, H.-Y. Ko, A. Kokalj, E. Küçükbenli, M. Lazzeri, M. Marsili, N. Marzari, F. Mauri, N. L. Nguyen, H.-V. Nguyen, A. O. de-la Roza, L. Paulatto, S. Poncé, D. Rocca, R. Sabatini, B. Santra, M. Schlipf, A. P. Seitsonen, A. Smogunov, I. Timrov, T. Thonhauser, P. Umari, N. Vast, X. Wu, and S. Baroni, J. Phys.: Condens. Matter **29**, 465901 (2017).

[43] P. E. Blöchl, Phys. Rev. B **50**, 17953 (1994).

[44] J. P. Perdew, K. Burke, and M. Ernzerhof, Phys. Rev. Lett. **77**, 3865 (1996).

[45] S. Grimme, J. Antony, S. Ehrlich, and H. Krieg, J. Phys. Chem. **132**, 154104 (2010).

[46] H. J. Monkhorst and J. D. Pack, Phys. Rev. B **13**, 5188 (1976).

[47] S. Nosé, J. Phys. Chem. **81**, 511 (1984).

[48] W. Hu, T. Wang, R. Zhang, and J. Yang, J. Mater. Chem. C **4**, 1776 (2016).

[49] W. Xiong, C. Xia, X. Zhao, T. Wang, and Y. Jia, Carbon **109**, 737 (2016).

[50] Z. Liu, J. Z. Liu, Y. Cheng, Z. Li, L. Wang, and Q. Zheng, Phys. Rev. B **85**, 205418 (2012).

[51] G. Graziano, J. Klimeš, F. Fernandez-Alonso, and A. Michaelides, J. Phys.: Condens. Matter **24**, 424216 (2012).

[52] W. Tang, E. Sanville, and G. Henkelman, J. Phys.: Condens. Matter **21**, 084204 (2009).

[53] J. Bardeen, Phys. Rev. **71**, 717 (1947).

[54] M. Sun, J.-P. Chou, Q. Ren, Y. Zhao, J. Yu, and W. Tang, Appl. Phys. Lett. **110**, 173105 (2017).

[55] M. Yankowitz, K. Watanabe, T. Taniguchi, P. San-Jose, and B. J. LeRoy, Nat. Commun. **7**, 1 (2016).

[56] P. K. Nayak, Y. Horbatenko, S. Ahn, G. Kim, J.-U. Lee, K. Y. Ma, A.-R. Jang, H. Lim, D. Kim, S. Ryu, H. Cheong, N. Park, and H. S. Shin, ACS Nano **11**, 4041 (2017).